J IRAN CHEM SOC (2014) 11:407–414
DOI 10.1007/s13738-013-0312-7

ORIGINAL PAPER

$Cu_3Mo_2O_9$ nanosheet incorporated with hemoglobin on carbon ionic liquid electrode for the direct electrochemistry and electrocatalysis

Liqi Zhang · Tongtong Li · Ying Deng · Yuanyuan Zhang · Song Hu · Wei Sun

Received: 19 September 2012 / Accepted: 9 July 2013 / Published online: 8 August 2013

Abstract In this paper $Cu_3Mo_2O_9$ nanosheet was prepared by a hydrothermal method and further used to investigate the direct electrochemistry of hemoglobin (Hb) with a carbon ionic liquid electrode (CILE) as the substrate electrode. Hb was mixed with $Cu_3Mo_2O_9$ nanosheet and cast on the CILE surface with chitosan (CTS) as the film-forming material. UV-vis and FT-IR spectroscopic results showed that Hb remained in its native structure in the composite film. Direct electron transfer of Hb on the modified electrode was realized with a pair of well-defined quasi-reversible redox waves that appeared on cyclic voltammograms. The redox peak potential appeared at −0.252 V (E_{pc}) and −0.141 V (E_{pa}), respectively, with the formal peak potential calculated as −0.196 V, which was the characteristic of electroactive center of Hb heme Fe(III)/Fe(II). The result could be attributed to the presence of $Cu_3Mo_2O_9$ nanosheet on the electrode surface that was of benefit for the protein orientation and promoted direct electron transfer between the redox active center of Hb and the substrate electrode. The CTS/$Cu_3Mo_2O_9$–Hb/CILE showed good electrocatalytic ability in reducing different substrates such as trichloroacetic acid, H_2O_2 and O_2, with wider linear range and lower detection limit, thus exhibiting the potential application of the $Cu_3Mo_2O_9$ nanosheet in third-generation electrochemical biosensors.

L. Zhang · S. Hu
State Key Laboratory of Coal Combustion, Huazhong University of Science and Technology, Wuhan 430074, People's Republic of China

T. Li · Y. Deng · Y. Zhang · W. Sun (✉)
College of Chemistry and Molecular Engineering, Qingdao University of Science and Technology, Qingdao 266042, People's Republic of China
e-mail: swyy26@hotmail.com

Keywords Electrochemical biosensor · Carbon ionic liquid electrode · Hemoglobin · $Cu_3Mo_2O_9$ nanosheet

Introduction

The investigation of direct electron transfer of redox proteins to the electrode is of great importance, and research can provide a mechanistic understanding of the electron transfer in biological systems [1]. Also the protein-modified electrodes can be used as third-generation electrochemical biosensors without mediators. But the direct transfer process cannot be realized on the commonly used solid electrode because of the deeply buried electroactive center of the protein and the unfavorable orientation of the protein structure on the electrode surface [2]. Therefore, different kinds of ultrathin films have been devised to immobilize the redox proteins on the electrode surface to achieve the electron transfer, which can provide a suitable microenvironment for retaining the protein structure and promoting the electron transfer rate between the proteins and the underlying electrode. The films can be prepared by insoluble surfactants, biopolymers, polyelectrolytes, nanomaterials, and organic–inorganic composite materials [3–5]. In recent years various kinds of nanoparticles have been widely used in the protein electrochemistry. Due to the specific properties of nanoparticles including bigger surface area, better biocompatibility and higher electrocatalytic activity, nanoparticles modified electrode can effectively accelerate the direct electrochemistry of redox proteins. A series of nanomaterials such as carbon nanotubes, graphene, metal nanoparticles, and semiconductors with different morphographies had been reported for the realization of the direct electron transfer between proteins and the underlying electrodes [6–10].

Ionic liquids (ILs) have exhibited some specific characteristics including high ionic conductivity, wide electrochemical windows and good solubility [11]. Carbon ionic liquid electrode (CILE) has been proposed as a new kind of chemically modified carbon paste electrode (CPE) with ILs as modifier and/or binder. By substituting the traditional liquid paraffin with ILs, CILE has exhibited many advantages such as high electronic conductivity, remarkable electrocatalytic activity, inexpensive reagents, easy fabrication, stable electrochemical responses and good anti-fouling ability [12, 13]. Sun et al. [14, 15] applied different CILEs to the detection of some electroactive substances such as DNA and catechol. Shiddiky [16] and Opallo [17] reviewed the application of ILs in the electrochemical sensing system. Recently, chemically modified CILE has also been prepared for the electrochemical sensor, which can combine the advantages of modifier and the CILE [7, 18]. Due to the excellent electrochemical characteristics of ILs including high ionic conductivity, wide electrochemical windows and good stability, ILs have been used in the protein electrochemistry as not only the supporting electrolyte but also the electrode modifier. Wang et al. investigated the direct electrochemistry of heme proteins in agarose hydrogel films with IL as the supporting electrolyte [19]. Safavi et al. [20] realized the direct electron transfer of Hb with a IL/CILE. IL can also be used as an enhancer in composite materials to enhance the direct electron transfer with different kinds of nanoparticles such as CoO nanoflower [21], CdS nanorod [22], carbon-coated Fe_3O_4 nanospindle [23], and graphene [24], which exhibited the synergistic effects with improved performances.

Molybdenum oxide-based materials are of contemporary interests due to their promising applications in the area of catalysis, absorption, electrical conductivity, magnetism, photochemistry, sensors and energy storage [25–27]. As one of molybdenum oxide-based minerals, the copper molybdate [$Cu_3Mo_2O_9$] was originally found in Chile and first described by Palache [28]. The properties of $Cu_3Mo_2O_9$ such as its crystal structure, Raman spectra, catalytic effect and thermal decomposition behavior have been widely investigated [29–31], which has attracted extensive interests in various research fields. Hasan et al. [32] applied $Cu_3Mo_2O_9$ for catalytic oxidation (combustion) of the emitted harmful gases such as CO, NO, and hydrocarbons. Vilmiont et al. [33] presented a hydrothermal synthesis of lindgrenite, and investigated its thermal, optical and magnetic properties. Bao et al. [34] synthesized $Cu_3(MoO_4)_2(OH)_2$ by hydrothermal method, which could be further transferred to metastable $Cu_3Mo_2O_9$ by thermal decomposition. Xu et al. [35] established a simple and mild hydrothermal route for the synthesis of lindgrenite with hollow and prickly sphere-like architecture, which was further processed by a simple thermal treatment to get the $Cu_3Mo_2O_9$ with the similar size and morphology. Jiang et al. [36] synthesized lindgrenite nanocrystals by simple aqueous precipitation, which could be decomposed to $Cu_3Mo_2O_9$. However, to our knowledge no documents reported using $Cu_3Mo_2O_9$ nanosheets to investigate direct electron transfer of Hb to CILE.

In this paper, an ionic liquid 1-hexylpyridinium hexafluorophosphate ($HPPF_6$) was selected as a binder to fabricate CILE and further used as the basal electrode for the electrochemical protein biosensor. Then $Cu_3Mo_2O_9$ nanosheets and Hb molecules were mixed together to form a novel bionanocomposite, which was immobilized on the CILE surface by the simple casting method. Chitosan (CTS) was further cast on the electrode to fix the nanocomposite tightly on the surface. CTS is an abundant natural cationic biopolymer with excellent characteristics such as film-forming ability, biocompatibility, nontoxicity, good water permeability, high mechanical strength and adhesion, which had been used in the chemically modified electrodes [37, 38]. The immobilized Hb retained its native structure in the composite film and the experimental results indicated that the electrochemical response of Hb was greatly enhanced with the appearance of a pair of well-defined quasi-reversible redox peaks. The modified electrode exhibited high electrocatalytic ability to the reduction of different substrates such as trichloroacetic acid, H_2O_2, and O_2, indicating the potential applications of $Cu_3Mo_2O_9$ nanosheet in the electrochemical sensors.

Experimental

Apparatus and chemicals

All the voltammetric measurements were performed on a CHI 1210A electrochemical workstation (Shanghai CH Instruments, China) and electrochemical impedance spectroscopy (EIS) was carried out on a CHI 750B electrochemical workstation (Shanghai CH Instruments, China). A three-electrode system was employed for the electrochemical investigation, which was composed of a modified CILE as working electrode, a Pt wire as auxiliary electrode and a saturated calomel electrode (SCE) as reference electrode. Ultraviolet-visible (UV-vis) absorption spectra and Fourier transform infrared (FT-IR) spectra were recorded on Cary 50 probe spectrophotometer (Varian Company, Australia) and Tensor 27 FT-IR spectrophotometer (Bruker Company, Germany), respectively. A scanning electron microscopy (SEM), JSM-6700F, was used to record the morphology (Japan Electron Company, Japan).

1-Hexylpyridinium hexafluorophosphate ($HPPF_6$, Lanzhou Greenchem. ILS. LICP. CAS., China), hemoglobin (Hb, MW. 64500, Sigma), graphite powder (average

particle size 30 μm, Shanghai Colloid Chemical Ltd. Co., China), trichloroacetic acid (TCA, Tianjin Kemiou Chemical Ltd. Co., China) and chitosan (CTS, Dalian Xindie Ltd. Co., China) were used as received. All of the other chemicals used were of analytical reagent grade and double-distilled water was used in the experiments.

Synthesis of $Cu_3Mo_2O_9$ nanosheets

$Cu_3Mo_2O_9$ nanosheets were synthesized at room temperature based on a procedure similar to the reference [35]. By carefully adding polyvinylpyrrolidone (PVP) (0.16 g) into $NaMoO_4$ solution (30.0 mL, 0.1 mol L^{-1}) with vigorous stirring for 30 min, $CuSO_4$ solution (30.0 mL, 0.1 mol L^{-1}) was added and continuously stirred for another 30 min. The as-prepared microemulsion mixture was then transferred into a stainless Teflon lined autoclave and heated at 110 °C for 12 h. The resulting suspension was naturally cooled to room temperature. The products were collected, centrifuged and washed with ethanol and water for several times, and then drying at 60 °C to get the $Cu_3(MoO_4)_2(OH)_2$. Finally, the products were annealed at 500 °C for 3 h to get the $Cu_3Mo_2O_9$ nanosheets, which was rinsed with distilled water and anhydrous alcohol at least five times, then centrifuged and dried for further use.

Preparation of the modified electrode

Based on the reported procedure [10], CILE was prepared with $HPPF_6$ and the surface of CILE was polished by smoothing on a weighing paper just before use. Typically a solution containing 15.0 mg mL^{-1} of Hb and 0.25 mg mL^{-1} $Cu_3Mo_2O_9$ nanosheets were mixed and shaken homogeneously. Then 8.0 μL of the prepared Hb–$Cu_3Mo_2O_9$ mixture was cast on the CILE surface and left to dry at room temperature. Finally 5.0 μL of 1.0 mg mL^{-1} CTS solution (in 1.0 % HAc) was spread onto the Hb–$Cu_3Mo_2O_9$ surface to form a stable film and the resulted electrode was denoted as CTS/Hb–$Cu_3Mo_2O_9$/CILE, which was stored at 4 °C when not in use.

Results and discussion

SEM of $Cu_3Mo_2O_9$ nanosheet

Scanning electron microscopy is an effective method for characterizing the morphology of the nanomaterials. The top SEM views of the synthesized $Cu_3Mo_2O_9$ were recorded and shown in Fig. 1, which clearly illustrated the typically two-dimensional sheets like structure with uniform distribution. The inset was the enlarged image, which indicated that $Cu_3Mo_2O_9$ existed as sheet with the sizes of 50–80 nm in thickness. The SEM image proved the successful synthesis of the $Cu_3Mo_2O_9$ nanosheets with uniform appearance and large surface area.

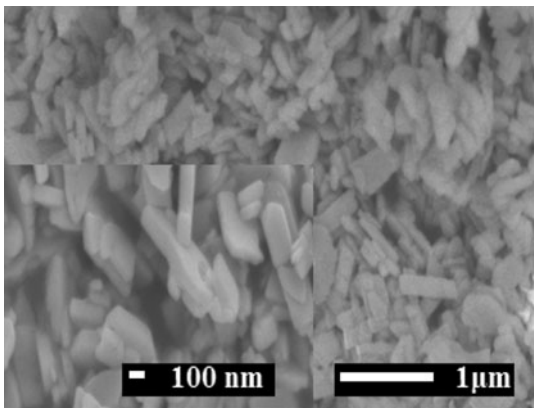

Fig. 1 SEM images of $Cu_3Mo_2O_9$ nanosheets with different scale

Spectroscopic results

Fourier transform infrared spectroscopy is commonly used to probe into the secondary structure of proteins. The shape and position of the amide I (1,700–1,600 cm^{-1}) and II (1,600–1,500 cm^{-1}) infrared absorbance bands of Hb can provide the detailed information on the secondary structure of the polypeptide chain. If Hb molecule is denatured, the intensity and shape of the amide I and II bands would diminish or disappear. FT-IR spectra of Hb and its mixture were recorded with the results shown in Fig. 2A. It can be seen that FT-IR peaks of these two amide bands of pure Hb molecules were located at 1,657.59 and 1,535.75 cm^{-1} (Fig. 2Aa). While FT-IR spectrum of CTS–Hb–$Cu_3Mo_2O_9$ mixture gave the position of the amide I and II bands at 1,655.44 and 1,533.92 cm^{-1} (Fig. 2Ab). The similar positions indicated that Hb retained the essential features of its native structure after mixing with the CTS and $Cu_3Mo_2O_9$ nanosheet.

In UV-vis absorption spectrum the Soret absorption band from the heme groups of Hb can provide the information on the conformational integrity of the proteins, the possible denaturation or the conformational change about the heme region. As shown in Fig. 2B, Hb had a Soret band at 405.9 nm in water (curve a) and 406.0 nm in 0.2 mol L^{-1} pH 3.0 PBS (curve b). After Hb was mixed with $Cu_3Mo_2O_9$ nanosheets in pH 3.0 PBS, the same absorption value of 406.0 nm appeared (curve c). The same position of the absorption peak also suggested that Hb retained its native structure in the mixture, which could be attributed to the biocompatibility of materials used.

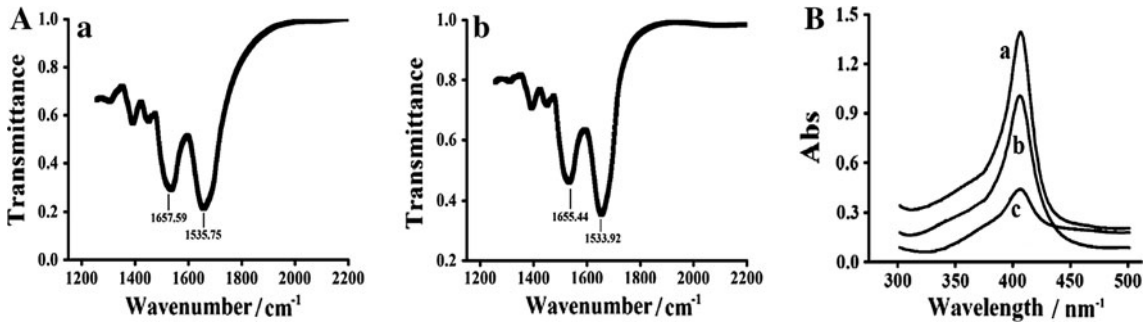

Fig. 2 **A** FT-IR spectra of *a* Hb and *b* CTS/$Cu_3Mo_2O_9$–Hb film; **B** UV-vis absorption spectra of Hb in water (*a*), Hb (*b*) and CTS-Hb-$Cu_3Mo_2O_9$ mixture solution (*c*) with pH 3.0 PBS

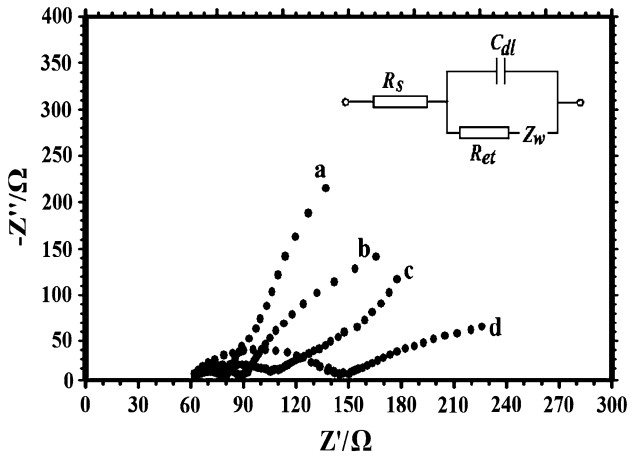

Fig. 3 Electrochemical impedance spectroscopy of *a* CILE, *b* CTS/CILE, *c* CTS/$Cu_3Mo_2O_9$–Hb/CILE, and *d* CTS/Hb/CILE in a 5.0 mmol L^{-1} $[Fe(CN)_6]^{3-/4-}$ + 0.1 mol L^{-1} KCl mixture solution with the frequencies ranging from 10^4 to 0.1 Hz. Inset is the Randles circuit

EIS of the modified electrodes

Electrochemical impedance spectroscopy is a powerful tool for studying the interfacial properties of the modified electrodes, which can provide information on the impedance changes of the electrode surface/electrolyte solution. The value of the electron transfer resistance (Ret) depends on the dielectric and insulating features at the electrode/electrolyte interface, which controls the electron transfer kinetics of the redox probe. The Nyquist plots of different modified electrodes were recorded and shown in Fig. 3, and the semicircle diameter of the curve was equal to the Ret. To get the detailed information the Randles circuit (shown as inset of Fig. 3) is chosen to fit the impedance data obtained. On bare CILE the Ret value was obtained as 18.72 Ω (curve a), and that of CTS/CILE increased to 29.87 Ω (curve b), which indicated that CTS film on the electrode acted as a blocking layer that could hinder the diffusion of ferricyanide toward the electrode surface. When Hb was entrapped in CTS film, the Ret value was further increased to 131.5 Ω (curve d), indicating that Hb molecules were successfully immobilized on the electrode surface and the presence of Hb further hindered the pathway of electron transfer. On CTS/Hb–$Cu_3Mo_2O_9$/CILE, the Ret value decreased to 41.87 Ω (curve c), indicating that $Cu_3Mo_2O_9$ nanosheets in the composite film could decreased the resistance. So the presence of $Cu_3Mo_2O_9$ nanosheets on the electrode surface can enhance the electron transfer rate of $[Fe(CN)_6]^{3-/4-}$ probe, which may be due to the increase of the surface area with certain conductivity.

Direct electrochemistry of Hb on the modified electrodes

Typical cyclic voltammograms of different modified electrodes were recorded in 0.1 mol L^{-1} pH 3.0 PBS with a scan rate of 100 mV s^{-1} and the results were shown in Fig. 4. No electrochemical responses could be observed CTS/CILE (curve c) in the potential range of investigation, which indicated that the electrode was stable and no electroactive substances existed on the electrode surface. While on CTS/Hb/CILE a pair of unsymmetric redox peaks appeared (curve b), indicating a quasi-reversible electrode process of Hb on CILE with slow electron transfer rate. The electrochemical data were obtained as 7.8 and 4.6 μA for the reduction peak current (I_{pc}) and the oxidation peak current (I_{pa}). In general direct electrochemistry of redox protein is often hard to be realized on the naked electrode due to the deep burying of the electroactive center in the protein structure or the unfavorable orientation on the electrode surface, which hindered the electron transfer rate. The incorporation of IL in the graphite powder could increase the interface conductivity and a layer of IL film was also present on the CILE surface, which was benefit for the electron transfer between Hb and CILE. So direct electron transfer of Hb was realized on CILE with slow rate. On CTS/Hb–$Cu_3Mo_2O_9$/CILE a pair of well-defined redox peaks appeared with more symmetric peak shape

(curve a). The values of I_{pc} and I_{pa} were obtained as 14.7 and 7.9 μA, which was bigger than that of CTS/Hb/CILE, indicating the electron transfer rate was enhanced. The results indicated that the presence of $Cu_3Mo_2O_9$ nanosheet in the composite film exhibited excellent ability to accelerate the electron transfer, which may be attributed to its high surface area and certain proton conductivity. The cathodic peak potential (E_{pc}) was located at −0.252 V and the anodic peak potential (E_{pa}) at –0.141 V. The apparent formal peak potential ($E^{0'}$), which is defined as the average value of E_{pc} and E_{pa}, [$E^{0'} = (E_{pc} + E_{pa})/2$], was estimated to be −0.196 V (vs. SCE). The result was the characteristic of a reversible electrode process of the heme Fe(III)/Fe(II) couple of the immobilized Hb molecules [39]. The peak-to-peak separation (ΔEp) was calculated as 111 mV at a scan rate of 100 mV s^{-1}, also indicating a quasi-reversible electron transfer process. So the presence of $Cu_3Mo_2O_9$ nanosheets on CILE surface could promote the direct electron transfer efficient of Hb due to its specific microstructure.

Cyclic voltammograms of CTS/Hb–$Cu_3Mo_2O_9$/CILE at different scan rates were recorded in pH 3.0 PBS with a pair of well-defined redox peaks appeared. The redox peak currents increased gradually with the increase of scan rate in the range from 100 to 400 mV s^{-1}. A good linear relationship could be established between the redox peak current and the scan rate with the linear regression equations as $I_{pc}(\mu A) = 1.45–56.54v$ (V s^{-1}) ($\gamma = 0.997$) and $I_{pa}(\mu A) = 12.16 + 64.99v$ (V s^{-1}) ($\gamma = 0.998$), which were the characteristics of a surface-confined thin-layer electrochemical behavior. So the electrochemically active Hb Fe(III) in the film on CILE surface was reduced to Hb Fe(II) on the forward scan,which was converted to Hb Fe(III) on the reverse scan. By integration of the cyclic voltammetric peaks of the modified electrode, the average surface coverage (Γ*) of electroactive Hb was estimated according to the following equation [40]: $Q = nFA\Gamma^*$, where Q is the charge passing through the electrode with full reduction of electroactive Hb in the film, n is the number of electrons transferred, F is the Faraday's constant, and A is the effective surface area of electrode. Based on the Randles-Sevcik equation: $I_{pc} = (2.69 \times 10^5)n^{3/2}AD^{1/2}Cv^{1/2}$, where I_{pc} is the reduction peak current (A), n is the electron transfer number, A is the electroactive surface area (cm^2), D is the diffusion coefficient of $K_3[Fe(CN)_6]$ in the solution (cm^2 s^{-1}), C is the concentration of $K_3[Fe(CN)_6]$ (0.1×10^{-3} mol cm^{-3}) and v is the scan rate (V s^{-1}), the electroactive surface area (A) of the electrode could be calculated as 0.126 cm^2. Then the surface concentration of electroactive Hb (Γ*) was calculated as 1.42×10^{-9} mol cm^{-2}. Because the total amount of Hb cast on the electrode surface was 1.47×10^{-8} mol cm^{-2}, the electroactive Hb on the electrode surface accounted for 9.66 % of the total amount of Hb in the film.

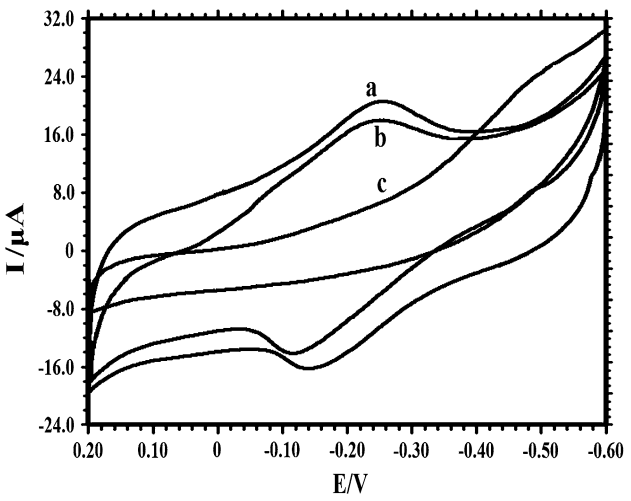

Fig. 4 Cyclic voltammograms of *a* CTS/$Cu_3Mo_2O_9$–Hb/CILE, *b* CTS/Hb/CILE, and *c* CTS/CILE in pH 3.0 PBS with the scan rate as 100 mV s^{-1}

The linear relationship between the redox peak potential with ln$v$ was also established with two straight lines obtained. The linear regression equations were got as $E_{pc}(V) = -0.03\ln v - 0.29$ ($\gamma = 0.997$) and $E_{pa}(V) = 0.019\ln v - 0.097$ ($\gamma = 0.998$). According to Laviron's equation, the values of the electron transfer coefficient (α), the electron transfer number (n) and the apparent heterogeneous electron transfer rate constant (k_s) were calculated as 0.7, 1.2, and 0.608 s^{-1}, respectively. The k_s value was much larger that of Hb immobilized on Nafion/DNA/CILE (0.31 s^{-1}) [41] and Ag/Ag_2O nanoparticles modified silver electrode (0.239 s^{-1}) [42], indicating a fast electron transfer process.

The effect of buffer pH on the cyclic voltammetric responses of the modified electrode was further investigated in the pH range from 2.0 to 8.0. A pair of redox peaks could be obtained and the formal peak potential ($E^{0'}$) of Hb shifted to the negative direction with the increase of buffer pH. A linear regression equation was obtained as $E^{0'}(V) = -0.0524$ pH + 0.061 ($n = 8$, $\gamma = 0.992$). The slope value of −52.4 mV pH^{-1} was a little smaller than the theoretically expected value of −59.0 mV pH^{-1} at 25 °C for a single proton coupled reversible one-electron transfer. The reason might be due to the influence of the protonation states of transligands to the heme ion and amino acids around the heme, or the protonation of the water molecule coordinated to the central ion. It also could be concluded that a single protonation accompanied with one electron transfer of Hb Fe(III) to electrode and the electrochemical reduction of Hb could be simply expressed as the following equation as Hb heme Fe(III) + H^+ + e^- → Hb heme Fe(II). Also the biggest redox peaks appeared at pH 3.0

buffer solution, which was selected as the experimental condition.

Electrocatalytic activity

Due to the catalytic properties of redox protein, electrocatalytic activity of Hb modified electrode to different substrates was carefully investigated. Trichloroacetic acid (TCA) is an analogue of acetic acid in which the three hydrogen atoms of the methyl group have been replaced by chlorine atoms. It is widely used in biochemistry for the precipitation of macromolecules and cosmetic treatments. It is also an environmental pollutant that can kill normal cells. So the determination of TCA has received great attentions in recent years [43, 44]. The electrocatalytic reduction of TCA on CTS/Hb–$Cu_3Mo_2O_9$/CILE was examined by cyclic voltammetry with the results shown in Fig. 5. After the addition of TCA into the deoxygenated pH 3.0 PBS, an obvious reduction peak appeared at −0.248 V with the decrease of the corresponding oxidation peak current, which was a typical electrocatalytic reaction. With the further increase of the TCA concentration, another reduction peak appeared at −0.48 V. Based on the reference [45], the second reduction peak could be tentatively assigned to the highly reduced form of Hb [Hb Fe(I)], which was an active reductant that could dechlorinate di- and monochloroacetic acid after the dechlorination of TCA by Hb Fe(II). The catalytic reduction peak currents increased with the TCA concentration in the range from 0.5 to 36.0 mmol L^{-1} with the linear regression equation as $I_{ss}(\mu A) = 4.08C$ (mmol L^{-1}) + 20.18 ($\gamma = 0.998$) and the detection limit was calculated as 0.16 mmol L^{-1} (3σ), which was lower than that of Nafion/nano-CdS/Hb/CILE (10.0 mmol L^{-1}) [22] and Nafion/Hb/CPE (5.6 mmol L^{-1}) [46]. When the TCA concentration was more than 36.0 mmol L^{-1}, an electrochemical response plateau appeared, indicating a typical Michaelis–Menten kinetic mechanism. So the apparent Michaelis–Menten constant (K_M^{app}) can be further calculated from the electrochemical version of Lineweaver–Burke equation. Based on the voltammetric results the value of K_M^{app} was calculated as 5.0 mmol L^{-1}, which was lower than the reported values of 47.0 mmol L^{-1} on Hb/agarose/GCE [19] and 90.8 mmol L^{-1} on Nafion-IL composite film modified CILE [3]. Since the K_M^{app} value is an indication of the enzyme-substrate kinetics, the smaller value indicates a high affinity of the enzyme with the substrate. So the fabricated electrode showed good electrocatalytic behavior to the reduction of TCA.

The CTS/$Cu_3Mo_2O_9$–Hb/CILE was further used to investigate its electrocatalytic activity to the reduction of H_2O_2 with the typical voltammograms shown in Fig. 6. The addition of H_2O_2 into PBS solution resulted in a new reduction peak at −0.38 V with the disappearance of the oxidation peak, which also indicated a typical electrocatalytic reaction. The reduction peak current increased with H_2O_2 concentration in the range from 0.4 to 198.0 μmol L^{-1} and the linear regression equation was calculated as $I_{ss}(\mu A) = 0.164C$ (μmol L^{-1}) + 66.92 ($n = 19$, $\gamma = 0.997$) with the detection limit as 0.13 μmol L^{-1} (3σ). The detection limit was much smaller than those obtained from Hb on the HRP/FMC–BSA/MWNTs/ormosil composite film modified electrode (5.0 μmol L^{-1}) [5] and the Hb–CILE (1.0 μmol L^{-1}) [47].

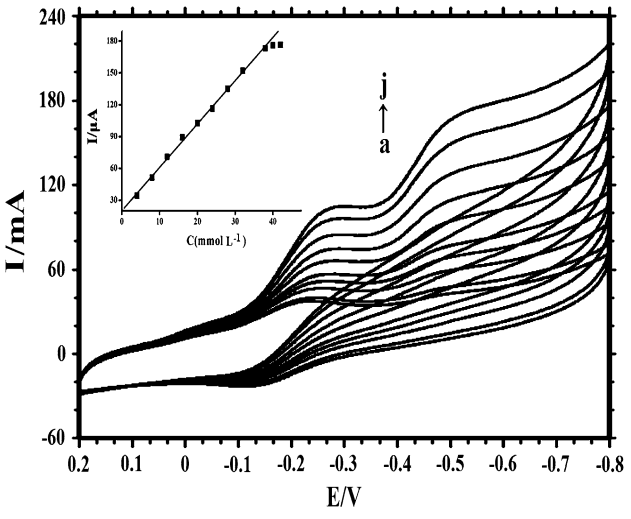

Fig. 5 Cyclic voltammograms of CTS/$Cu_3Mo_2O_9$–Hb/CILE in the presence of different concentration of TCA (from *a* to *j* 1.0, 2.0, 6.0, 10.0, 14.0, 20.0, 24.0, 28.0, 32.0, 34.0 mmol L^{-1}) with the scan rate as 100 mV s^{-1}. Inset was the linear relationship of catalytic reduction peak currents and the TCA concentration

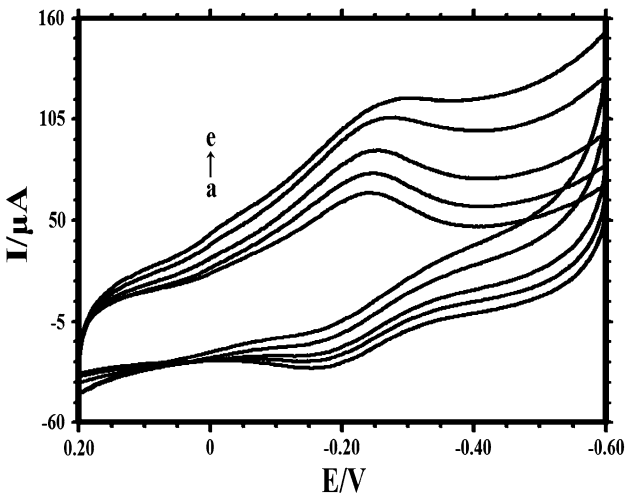

Fig. 6 Cyclic voltammograms of CTS/$Cu_3Mo_2O_9$–Hb/CILE in the presence of different concentration of H_2O_2 (from *a* to *e* are 0.0, 30.0, 100.0, 180.0, 280.0 μmol L^{-1}) with the scan rate as 100 mV s^{-1}

Table 1 Determination results of H_2O_2 in disinfector samples ($n = 3$)

Sample	Detected (mmol L^{-1})	Added (mmol L^{-1})	Total (mmol L^{-1})	Recovery[a] (%)	RSD (%)
1	0.42	0.40	0.83	103	3.48
2	0.47	0.80	1.32	106	2.87
3	0.44	1.00	1.42	98	3.05

[a] Recovery = (total − detected)/added × 100 %

When the H_2O_2 concentration was more than 200.0 μmol L^{-1}, the current response turned to level off, which indicated a saturation of Hb catalytic reaction. The apparent Michaelis–Menten constant (K_M^{app}) was further calculated as 0.24 mmol L^{-1}, which was smaller than that on Hb/Chit-Aus/Cys/Au electrode (1.4 mmol L^{-1}) [4], Au/cysteamine/Au electrode (2.3 mmol L^{-1}) [48] and sol–gel gold nanotubes (7.6 mmol L^{-1}) [49], indicating an obvious stronger interaction of Hb with H_2O_2.

The CTS/$Cu_3Mo_2O_9$–Hb/CILE was also exhibited excellent electrocatalytic ability to the reduction of O_2. Upon the injection of different amounts of air into the previously deoxygenated PBS by a syringe, the catalytic reduction peak current increased greatly with the decrease of the oxidation peak. The reduction peak current increased with the mount of air injected, which also indicated the prepared electrode could be used as the sensor for the detection of O_2 due to the presence of Hb on the electrode surface.

Analytical application

The fabricated electrode was applied to detect the H_2O_2 concentration in the real sample of disinfector that manufactured by Shandong Lircon Disinfection Technology Ltd. Co.. Under the selected conditions and by using the standard addition method, the determination results by the modified electrode were summarized in Table 1. It can be seen that the results were satisfactory with the recoveries in the range of 98–106 %, indicating the practical application of this electrode.

Stability and reproducibility of the modified electrode

The reproducibility of CTS/$Cu_3Mo_2O_9$–Hb/CILE was performed by measuring the current response of the electrode upon the addition of 1.0 mmol L^{-1} TCA with the average relative standard deviation (RSD) smaller than 3.5 %. In a series of 10 electrodes prepared in the same procedure, a RSD value of 2.85 % was obtained, indicating the repeatability of this method. In order to investigate the stability of the modified electrode, the current response to the detection of 1.0 mmol L^{-1} of TCA was recorded every 1 week. After 4 weeks storage it was found that the current could retain 93.6 % of its original signal, which showed long-term stability of the modified electrode.

Conclusions

In the present work $Cu_3Mo_2O_9$ nanosheets were synthesized and used to realize the direct electrochemistry of Hb with CILE as the substrate electrode. Electrochemical responses of Hb were realized and enhanced due to the presence of $Cu_3Mo_2O_9$ nanosheet with the electrochemical parameters calculated. The prepared CTS/$Cu_3Mo_2O_9$–Hb/CILE showed good stability to keep the bioactivity of Hb and the electrocatalysis of Hb-modified electrode to different substrates was achieved with wider linear range and lower detection limit.

Acknowledgments We acknowledge the financial support of the National Natural Science Foundation of China (No. 50976043, 51076056), the Foundation of State Key Laboratory of Coal Combustion of Huazhong University of Science and Technology (FSKLCC1010) and the Foundation of State Key Laboratory of Clean Energy Utilization of Zhejiang University.

References

1. J.F. Rusling, Acc. Chem. Res. **31**, 363 (1998)
2. F.A. Armstrong, G.S. Wilson, Electrochim. Acta **45**, 2623 (2000)
3. W. Sun, X.Q. Li, K. Jiao, Electroanalysis **21**, 959 (2009)
4. J.J. Feng, G. Zhao, J.J. Xu, H.Y. Chen, Anal. Biochem. **342**, 280 (2005)
5. V.S. Tripathi, V.B. Kandimalla, H.X. Ju, Biosens. Bioelectron. **21**, 1529 (2006)
6. P.A. Prakash, U. Yogesuwaran, S.M. Chen, Talanta **78**, 1414 (2009)
7. W. Sun, Y.Q. Guo, X.M. Ju, Y.Y. Zhang, X.Z. Wang, Z.F. Sun, Biosens. Bioelectron. **42**, 207 (2013)
8. C.L. Xiang, Y.J. Zou, L.X. Sun, F. Xu, Talanta **74**, 206 (2007)
9. W. Sun, L.F. Li, B.X. Lei, T.T. Li, X.M. Ju, X.Z. Wang, G.J. Li, Z.F. Sun, Mater. Sci. Eng. C **33**, 1907 (2013)
10. Z.Y. Zhao, L.L. Cao, A.H. Hu, W.L. Zhang, X.M. Ju, Y.Y. Zhang, W. Sun, Bull. Korean Chem. Soc. **34**, 475 (2013)
11. D. Wei, A. Ivaska, Anal. Chim. Acta **607**, 126 (2008)
12. N. Maleki, A. Safavi, F. Tajabadi, Anal. Chem. **78**, 3820 (2006)
13. M. Musameh, J. Wang, Anal. Chim. Acta **606**, 45 (2008)
14. W. Sun, Y.Z. Li, M.X. Yang, S.F. Liu, K. Jiao, Electrochem. Commun. **10**, 298 (2008)
15. W. Sun, Y.Z. Li, M.X. Yang, J. Li, K. Jiao, Sens. Actuators B Chem. **133**, 387 (2008)

16. M.J.A. Shiddiky, A.A.J. Torriero, Biosens. Bioelectron. **26**, 1775 (2011)
17. M. Opallo, A. Lesniewski, J. Electroanal. Chem. **656**, 2 (2011)
18. W. Sun, P. Qin, R.J. Zhao, K. Jiao, Talanta **80**, 2177 (2010)
19. S.F. Wang, T. Chen, Z.L. Zhang, X.C. Shen, Z.X. Lu, D.W. Pang, Langumir **21**, 9260 (2005)
20. A. Safavi, N. Maleki, O. Moradlou, M. Sorouri, Electrochem. Commun. **10**, 420 (2008)
21. Z.H. Zhu, X. Li, Y. Zeng, W. Sun, W. Zhu, X.T. Huang, J. Phys. Chem. C **25**, 12547 (2011)
22. W. Sun, D.D. Wang, G.C. Li, Z.Q. Zhai, R.J. Zhao, K. Jiao, Electrochim. Acta **53**, 8217 (2008)
23. Y. Ke, Y. Zeng, X.L. Pu, X. Wu, L.F. Li, Z.H. Zhu, RSC Adv. **2**, 5676 (2012)
24. L. Wang, X.H. Zhang, H.Y. Xiong, S.F. Wang, Biosens. Bioelectron. **26**, 991 (2010)
25. X. Cui, S. Yu, L. Li, L. Biao, H. Li, M. Mo, X. Liu, Chem. Eur. J. **10**, 218 (2004)
26. Y. Cheng, Y. Wang, D. Chen, F. Bao, J. Phys. Chem. B **109**, 794 (2005)
27. C. Canevali, F. Morazzoni, R. Scotti, D. Cauzzi, P. Moggic, G. Predieri, J. Mater. Chem. **9**, 507 (1999)
28. C. Palache, Am. Mineral. **20**, 484 (1935)
29. L.D. Calvert, W.H. Barnes, Can. Mineral. **6**, 31 (1957)
30. F.C. Hawthorne, R.K. Eby, Neues Jb. Miner. Monats **5**, 234 (1985)
31. R.L. Frost, L. Duong, M. Weler, Neues Jb. Miner. Abh. **180**, 245 (2004)
32. M.A. Hasan, M.I. Zaki, K. Kumari, L. Pasuputely, Thermochim. Acta **320**, 23 (1998)
33. S. Vilminot, G. Andre, M.R. Plouet, F.B. Vigneron, M. Kurmoo, Inorg. Chem. **45**, 10938 (2006)
34. R.L. Bao, Z.P. Kong, M. Gu, B. Yue, Chem. Res. Chin. Univ. **6**, 679 (2006)
35. J.S. Xu, D.F. Xue, Solid State Chem. **180**, 119 (2007)
36. J.W. Jiang, J. Fang, Z.Y. Fan, X.J. Yang, Q.T. Lu, Y.B. Hou, J. Inorg. Mater. **26**, 438 (2011)
37. Y. Liu, M. Wang, F. Zhao, Z. Xu, S. Dong, Biosens. Bioelectron. **21**, 984 (2005)
38. J. Tkac, J.W. Whittaker, T. Ruzgas, Biosens. Bioelectron. **22**, 1820 (2007)
39. H. Zhang, H.Y. Lu, N.F. Hu, J. Phys. Chem. B **110**, 2171 (2006)
40. A.J. Bard, L.R. Faulkner, *Electrochemical Methods* (Wiley, New York, 1980)
41. W. Sun, Y. Wang, X.Q. Li, J. Wu, T.R. Zhan, K. Jiao, Electroanalysis **21**, 2454 (2009)
42. Y.H. Wang, H.Y. Gu, Microchim. Acta **164**, 41 (2009)
43. T.A. Piggot, R.W. Norris, Br. J. Plast. Surg. **41**, 112 (1988)
44. H.K. Bhat, M.F. Kanz, G.A. Campbell, G.A.S. Ansari, Fundam. Appl. Toxicol. **17**, 240 (1991)
45. X. Ma, X.J. Liu, H. Xiao, G.X. Li, Biosens. Bioelectron. **20**, 1836 (2005)
46. W. Sun, Z.Q. Zhai, K. Jiao, Anal. Lett. **41**, 2819 (2008)
47. W. Sun, R.F. Gao, X.Q. Li, D.D. Wang, M.X. Yang, K. Jiao, Electroanalysis **20**, 1048 (2008)
48. Y. Xiao, H.X. Ju, H.Y. Chen, Anal. Biochem. **278**, 22 (2000)
49. M. Delvaux, A. Walcarius, S. Demoustier-Champagne, Anal. Chim. Acta **525**, 221 (2004)